



CFD modeling of condensation process of water vapor in supersonic flows

Yang, Yan ; Walther, Jens Honore; Yan, Yuying; Wen, Chuang

Published in:
Applied Thermal Engineering

Link to article, DOI:
[10.1016/j.applthermaleng.2017.01.047](https://doi.org/10.1016/j.applthermaleng.2017.01.047)

Publication date:
2017

Document Version
Peer reviewed version

[Link back to DTU Orbit](#)

Citation (APA):
Yang, Y., Walther, J. H., Yan, Y., & Wen, C. (2017). CFD modeling of condensation process of water vapor in supersonic flows. *Applied Thermal Engineering*, 115, 1357-1362.
<https://doi.org/10.1016/j.applthermaleng.2017.01.047>

General rights

Copyright and moral rights for the publications made accessible in the public portal are retained by the authors and/or other copyright owners and it is a condition of accessing publications that users recognise and abide by the legal requirements associated with these rights.

- Users may download and print one copy of any publication from the public portal for the purpose of private study or research.
- You may not further distribute the material or use it for any profit-making activity or commercial gain
- You may freely distribute the URL identifying the publication in the public portal

If you believe that this document breaches copyright please contact us providing details, and we will remove access to the work immediately and investigate your claim.

1 **CFD modeling of condensation process of water vapor in**
2 **supersonic flows**

3 Yan Yang^a, Jens Honore Walther^{b, c}, Yuying Yan^d, Chuang Wen^{a, b, *}

4 ^a School of Petroleum Engineering, Changzhou University, Changzhou, 213016,
5 China

6 ^b Section of Fluid Mechanics, Coastal and Maritime Engineering, Department of
7 Mechanical Engineering, Technical University of Denmark, Nils Koppels Allé, 2800
8 Kgs. Lyngby, Denmark

9 ^c Chair of Computational Science, ETH Zürich, Clausiusstrasse 33 ETH-Zentrum,
10 CLT F 11, CH-8092 Zürich, Switzerland

11 ^d Faculty of Engineering, University of Nottingham, University Park, Nottingham
12 NG7 2RD, UK

13 *Corresponding author: Chuang Wen, Email: cwen@mek.dtu.dk

14 **Abstract:** The condensation phenomenon of vapor plays an important role in various
15 industries, such as the steam flow in turbines and refrigeration system. A
16 mathematical model is developed to predict the spontaneous condensing phenomenon
17 in the supersonic flows using the nucleation and droplet growth theories. The
18 numerical approach is validated with the experimental data, which shows a good
19 agreement between them. The condensation characteristics of water vapor in the
20 Laval nozzle are described in detail. The results show that the condensation process is
21 a rapid variation of the vapor-liquid phase change both in the space and in time. The
22 spontaneous condensation of water vapor will not appear immediately when the steam

23 reaches the saturation state. Instead, it occurs further downstream the nozzle throat,
24 where the steam is in the state of supersaturation.

25 **Keywords:** condensation; water vapor; Laval nozzle; supersonic flow

26 **1. Introduction**

27 The condensation phenomenon of vapor plays an important role in various
28 industries, such as the steam flow and water vapor in nozzles [1], turbines [2], ejectors
29 [3], thermos-compressors [4] and supersonic separators [5-9]. Theoretical and
30 experimental studies have been conducted for the condensation process in supersonic
31 flows, focusing on the nucleation theory, droplet size, latent heat [10-12]. Numerical
32 simulations have been performed to predict the condensing flow with the
33 development of the computational fluid dynamics (CFD) for several decades.

34 Hill [13], Noori Rahim Abadi et al. [14] studied the nucleation process of wet
35 steam flows in nozzles at low and high pressure, respectively. White & Young
36 predicted the condensing process using Eulerian-Lagrangian and time-marching
37 methods [15]. Gerber [16] developed the Eulerian-Lagrangian and Eulerian-Eulerian
38 two-phase models for predicting the condensation flow with the classical nucleation
39 theory. The effects of friction factor on the condensation flows in the Laval nozzles
40 were performed using the single fluid model by Mahpeykar & Teymourash [17], and
41 Jiang et al. [18]. Two-dimensional simulation of the condensing steam was calculated
42 in converging-diverging nozzles using a Jameson-style finite volume method on an
43 unstructured and adaptive triangular mesh [19]. Yang & Sheng [20] described a
44 conservative two-dimensional compressible numerical model for the non-equilibrium

45 condensing of the steam flow based on the classical nucleation theory and the Virial
46 type equation of state. The effect of the expansion rate on the steam condensing flow
47 through a converging-diverging nozzle was studied numerically by Nikkhahi et al.
48 [21]. The steam condensing flow was modeled through the Laval nozzles at low and
49 high inlet pressures by means of the single-fluid model [22]. The Eulerian-Eulerian
50 approach was adopted for modeling the condensing steam flow, and the simulation
51 was conducted on the commercial ANSYS FLUENT 12.1 platform [23].

52 The condensation phenomenon of water vapor in supersonic flows is still not
53 understood very well as a result of the complex phase change process. Especially, the
54 numerical simulation depends on various nucleation theories and droplet growth
55 models. In this paper, the Euler-Euler two-phase flow model is developed to predict
56 the spontaneous condensing phenomenon in the Laval nozzle. The modified internally
57 consistent classic nucleation theory and Gyarmathy's droplet growth model are
58 employed to perform the simulation cases. The numerical approach is validated with
59 experimental data. The condensation process of water vapor is numerically analyzed
60 in detail, including the nucleation rate, droplet numbers, droplet radius and droplet
61 fraction.

62 **2. Mathematical model**

63 *2.1. Governing equations*

64 For the water vapor condensation in a Laval nozzle, the fluid flow is governed by
65 partial differential equations describing the conservation of mass, momentum and
66 energy, as shown in Eqs. (1-3).

$$67 \quad \frac{\partial \rho}{\partial t} + \frac{\partial(\rho u_j)}{\partial x_j} = S_m \quad (1)$$

$$68 \quad \frac{\partial}{\partial t}(\rho u_i) + \frac{\partial}{\partial x_j}(\rho u_j u_i) = -\frac{\partial p}{\partial x_i} + \frac{\partial \tau_{ij}}{\partial x_j} + S_{u_i} \quad (2)$$

$$69 \quad \frac{\partial}{\partial t}(\rho H) + \frac{\partial}{\partial x_j}(\rho u_j H + p) = -\frac{\partial}{\partial x_j}(\lambda_{eff} \frac{\partial T}{\partial x_j}) + \frac{\partial}{\partial x_j}(u_i \tau_{ij}) + S_{h_i} \quad (3)$$

70 where ρ , u , p and H are the density, velocity, pressure and total enthalpy, respectively.
 71 λ_{eff} and T are the effective heat conductivity and temperature. The source terms, S_m ,
 72 S_{u_i} , S_{h_i} , are needed in these equations to consider the effect of the condensation
 73 process.

74 Additionally, two transport equations are employed to describe the phase change
 75 process during the condensation of the water vapor. In this simulation, the
 76 conservation equations include the liquid fraction (Y) and droplet number (N), which
 77 can be given by:

$$78 \quad \frac{\partial(\rho Y)}{\partial t} + \frac{\partial}{\partial x_j}(\rho Y u_j) = S_Y \quad (4)$$

$$79 \quad \frac{\partial(\rho N)}{\partial t} + \frac{\partial}{\partial x_j}(\rho N u_j) = \rho J \quad (5)$$

80 where the source term S_Y describes the condensation rate of the water vapor, and J is
 81 the nucleation rate, respectively.

82 The source term can be defined as follows:

$$83 \quad S_m = -S_Y = -\dot{m} \quad (6)$$

$$84 \quad S_{u_i} = -\dot{m} u_i \quad (7)$$

$$85 \quad S_{h_i} = -\dot{m} h_i \quad (8)$$

86
$$\dot{m} = \frac{4\pi r^{*3}}{3} \rho_l J + 4\pi r^2 \rho_l N \frac{dr}{dt} \quad (9)$$

87 where \dot{m} is the condensation mass per unit vapor volume per unit time. ρ_l is the
 88 droplet density, r is the droplet radius. dr/dt is the growth rate of droplets. The r^* is the
 89 Kelvin-Helmholtz critical droplet radius, which can be given by

90
$$r^* = \frac{2\sigma}{\rho_l R_v T \ln(S)} \quad (10)$$

91 where S is the super saturation ratio, defined as the ratio of vapor pressure to the
 92 equilibrium saturation pressure.

93 The nucleation rate, J , can be calculated by the internally consistent classic
 94 nucleation theory (ICCT) [24], which predicts the nucleation process of the water
 95 vapor as follows:

96
$$J = \frac{\zeta}{S} \frac{\rho_v^2}{\rho_l} \sqrt{\frac{2\sigma}{\pi m_v^3}} \exp\left(-\frac{16\pi}{3} \frac{\sigma^3}{k_B^3 T_v^3 \rho_l^2 (\ln S)^2}\right) \exp(\Theta) \quad (11)$$

97 where σ is the liquid surface tension, m_v is the mass of a vapor molecule, k_B is the
 98 Boltzmann's constant, T_v is the vapor temperature, ζ is a correction factor, Θ is a
 99 dimensionless surface tension.

100
$$\Theta = \frac{\sigma a_0}{k_B T_v} \quad (12)$$

101 where a_0 is the molecular surface area.

102 The growth rate of droplets due to evaporation and condensation, dr/dt , is
 103 calculated by Gyarmathy's model by [25],

104
$$\frac{dr}{dt} = \frac{\lambda_v (T_s - T_v)}{\rho_l h} \frac{(1 - r^*/r)}{\left(r + \frac{\sqrt{8\pi}}{1.5 \text{Pr}} \frac{\gamma}{\gamma + 1} l\right)} \quad (13)$$

105 where λ_v is the heat conductivity coefficient of the vapor, h is the vapor specific
106 enthalpy, T_s is the saturated steam temperature, γ is the vapor adiabatic exponent, Pr is
107 the Prandtl number.

108 *2.2. Turbulence model*

109 Depending on the information required, different turbulence models can be
110 applied for the numerical simulation of supersonic flows, from k - ε model [26-28],
111 Shear Stress Turbulent (SST) k - ω [29], Large Eddy Simulation (LES) to Direct
112 Numerical Simulation (DNS). In this paper, the k - ε turbulence model is used to
113 predict the supersonic flows. The equations for the turbulence model are not
114 documented here for brevity, but are however well documented elsewhere [30].

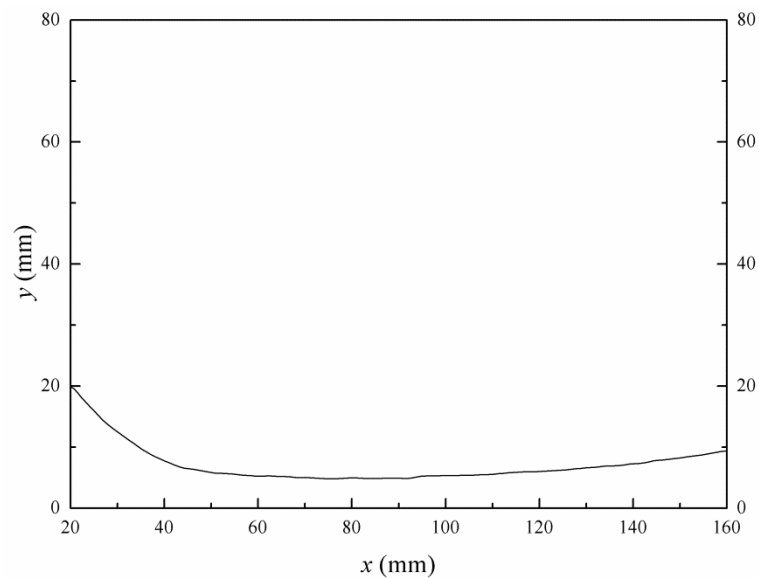
115 *2.3. Numerical schemes*

116 The commercial package ANSYS FLUENT 17 is employed as the computational
117 platform. The conservation equations (1)-(3) for vapor phase are directly solved in
118 FLUENT, while the governing equations (4)-(13) for liquid phase and the source
119 terms are performed with C code by the User-Defined-Scalar (UDS) and
120 User-Defined-Function (UDF) interfaces. The SIMPLE algorithm [31] is used to
121 couple the velocity field and pressure. The second-order upwind scheme is adopted
122 for an accurate prediction. The transient state solution is used in the numerical studies
123 with a time step of 10^{-6} s. The inlet conditions for the nozzle entrance are chosen from
124 experimental tests including total pressure and total temperature. Since the flow is
125 supersonic at the nozzle outlet, the pressure at the outlet does not influence the
126 solution and is assigned an arbitrary low value. The convergence criterion for the

127 relative residual of the continuity and all other dependent variables is set to 10^{-3} and
128 10^{-6} , respectively. The mass imbalance value is assigned as 10^{-4} to ensure iteration
129 convergence.

130 3. Results and discussion

131 The validation, verification and implementation of the numerical studies are
132 conducted using the geometry and experimental data from the available literature by
133 Moses & Stein [12]. In their studies, the Laval nozzle was employed to
134 experimentally study the condensation process of water vapor in supersonic flows.
135 The nozzle throat is located at $x=82.2$ mm with the dimension of 10.0 mm (height) \times
136 10.0 mm (depth). A sketch of the geometry of the Laval nozzle used in the
137 experiments is described in Fig. 1. The subsonic part is composed of an arc with a
138 radius of 53.0 mm, while the transonic and supersonic parts consist of an arc with a
139 radius of 686.0 mm.



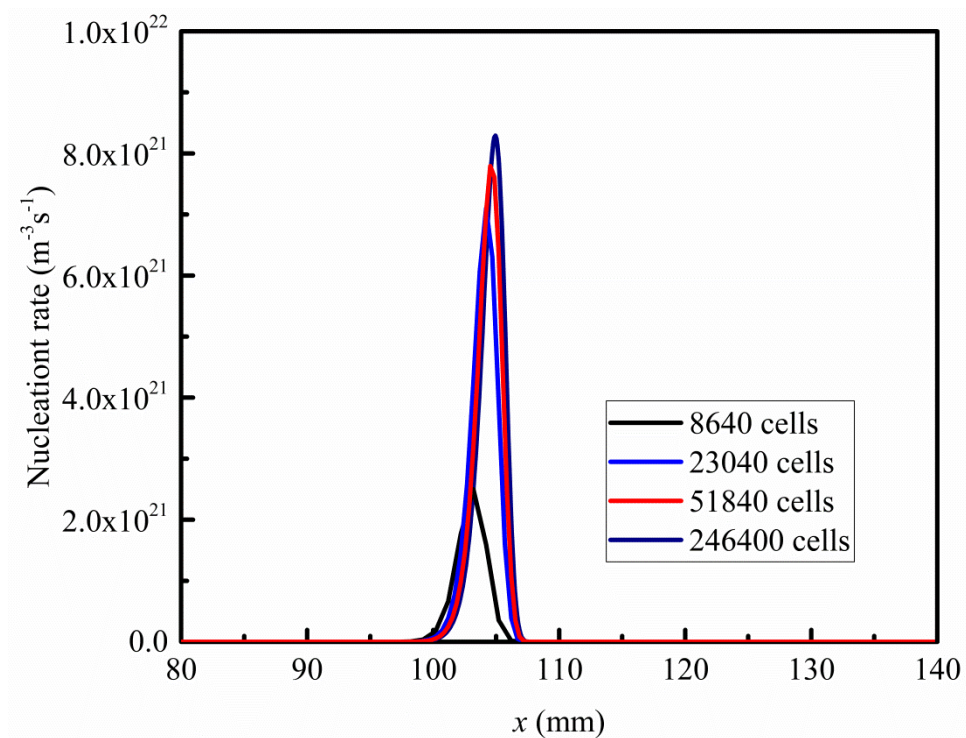
140

141

Fig. 1 Geometry and size of the Laval nozzle

142 3.1. Grid independence tests

143 The grid density is one of the key factors that determines the accuracy of the
144 numerical simulation. Three different densities of the structural grids are used to test
145 the grid independence, including the coarse (8640 cells), medium (23040 cells), fine
146 (51840 cells) and very fine (246400) grids. The static pressure and temperature at the
147 nozzle inlet for the simulations are 54702.17 Pa and 373.15 K, respectively. One of
148 the condensation parameters, the nucleation rate, is selected to evaluate the effect of
149 the grid density on the condensation simulation. The nucleation rate along the axis of
150 the Laval nozzle is shown in Fig. 2. We can see that the nucleation rate calculated
151 from the coarse grid significantly deviates from other cases, while the medium, fine
152 and very fine grids represent similar results. Therefore, the grid system with 23040
153 cells is used to conduct our simulations considering the computing accuracy and
154 efficiency.



155

156

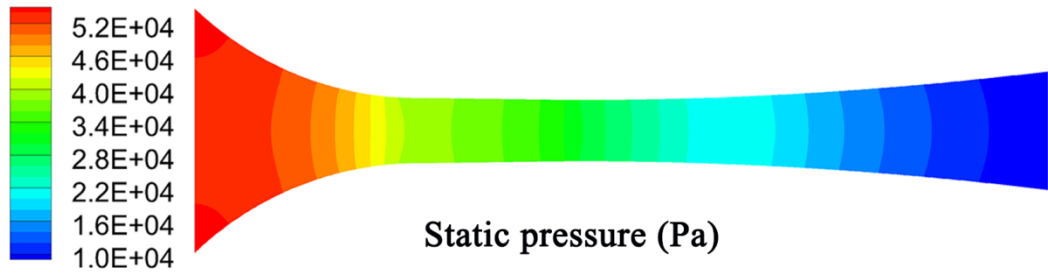
Fig. 2 Effect of grid density on nucleation rate in supersonic flows

157 *3.2. Model validation*

158 The static pressure is firstly compared between the numerical and experimental
159 data at the inlet pressure of 54702.17 Pa and inlet temperature of 373.15 K. The
160 numerical result of the static pressure is shown in Fig. 3, and the value at the central
161 line is employed for the data validation. Fig. 4 depicts the dimensionless pressure,
162 defined as the ratio of local static pressure to the inlet one, along the central axis of
163 the Laval nozzle. We can see that the predicted onset of the condensation process at
164 $x=104$ mm, occurs earlier than the experimental test at $x=107$ mm. The increase of the
165 static pressure due to the condensing flow in the simulation is smaller than the
166 experiments.

167 Then, the droplet fraction due to the condensation process is employed to
168 validate the numerical model. The pressure and temperature at the nozzle inlet are
169 40050.04 Pa and 374.30 K, respectively. Fig. 5 shows the numerical and experimental
170 data of the droplet fraction along the axis in the Laval nozzle. The numerical model
171 predicts the droplet fraction in supersonic flows, although almost all of the numerical
172 results are less than the experimental data.

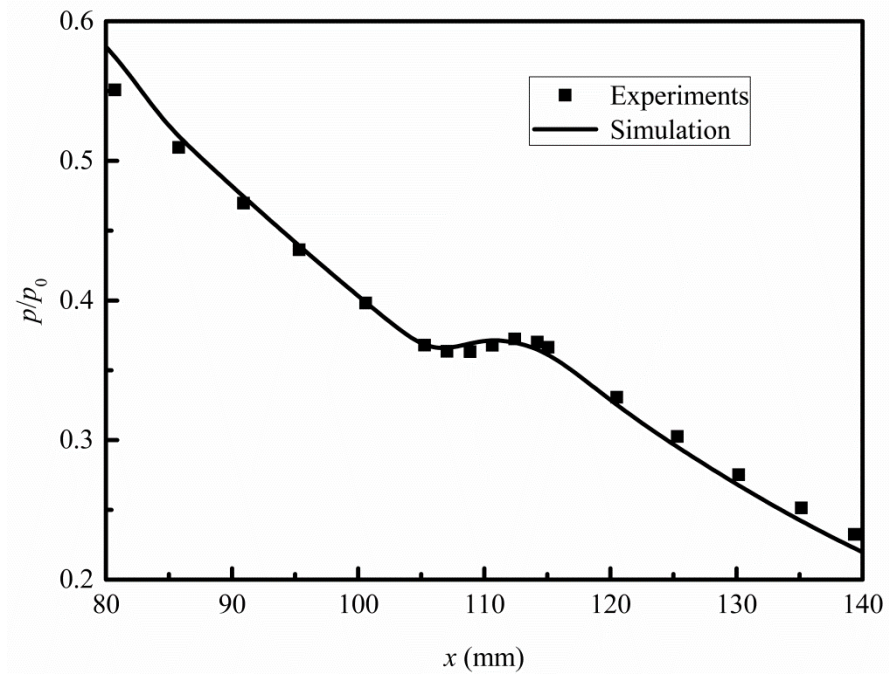
173 Generally, the numerical model is validated in detail by comparing the static
174 pressure and droplet fraction during the condensation process in the Laval nozzle. The
175 comparison results demonstrate that the numerical model can accurately capture the
176 condensation process of the water vapor in the Laval nozzle.



177

178

Fig. 3 Numerical results of static pressure in the Laval nozzle



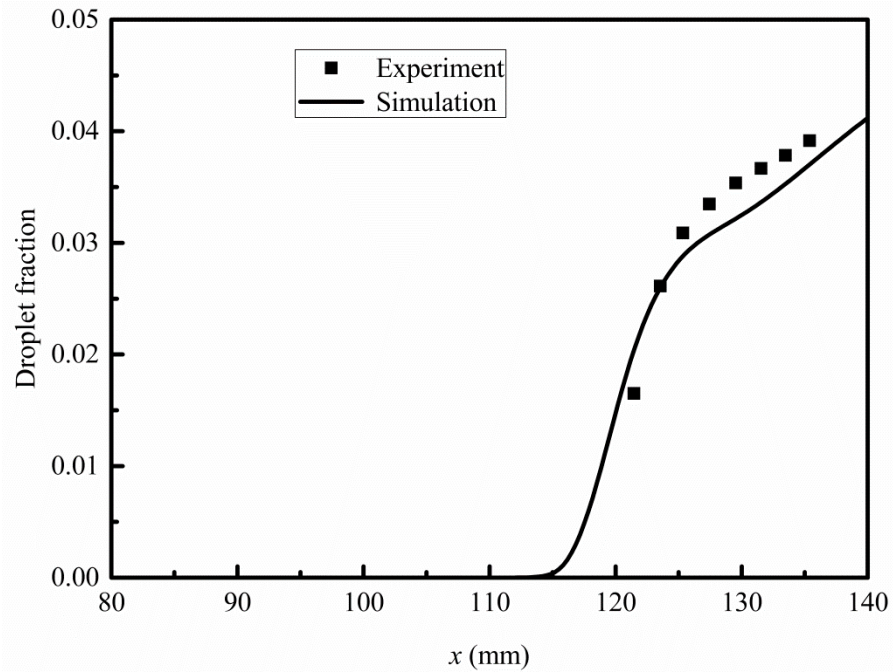
179

180

Fig. 4 Numerical and experimental results of static pressure at the central line of

181

the Laval nozzle

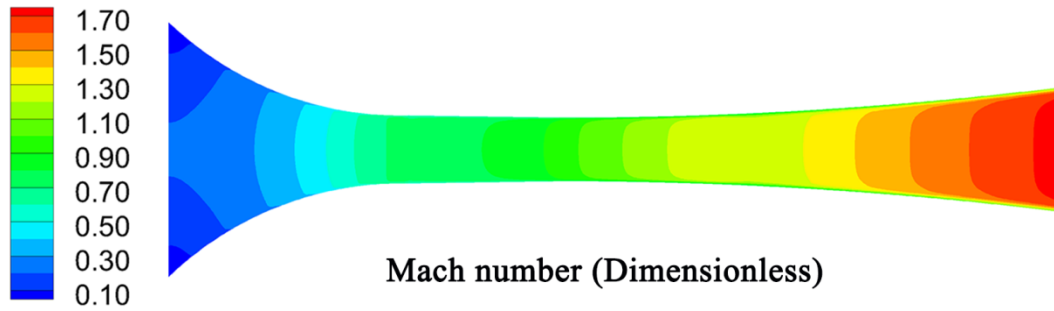


182

183 Fig. 5 Numerical and experimental results of droplet fraction at the central line of
 184 the Laval nozzle

185 *3.3. Condensation process*

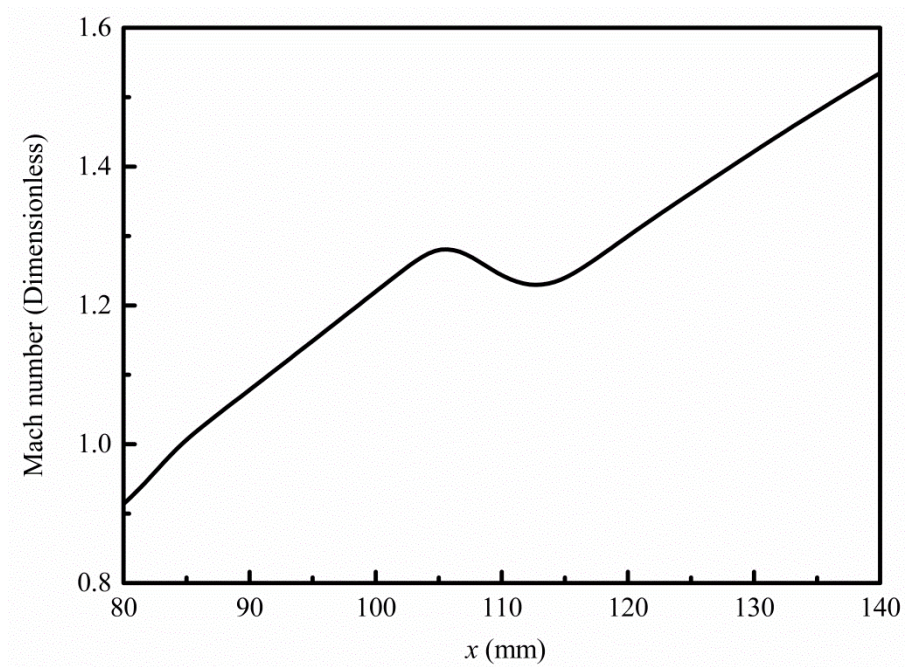
186 In this section, the condensation process of the water vapor is numerically
 187 calculated in the above mentioned Laval nozzle at the inlet pressure of 54702.17 Pa
 188 and temperature of 373.15 K, respectively. Fig. 6 shows the computational contours of
 189 the Mach number in the Laval nozzle, and the detailed information at the center line is
 190 described in Fig. 7. It can be observed that the vapor accelerates to a supersonic speed
 191 and correspondingly results in the increase of the Mach number. However, the Mach
 192 number starts to decrease, when the spontaneous condensation of water vapor occurs.
 193 This can be explained that the change of the latent heat between the phase transition
 194 process from the vapor to liquid will heat the water vapor. After that, the steam
 195 expands again, and the Mach number increases in the diverging part of the Laval
 196 nozzle.



197

198

Fig. 6 Mach number contours in the Laval nozzle



199

200

Fig. 7 Mach number at the central line of the Laval nozzle

201

Figs. 8 and 9 show the degree of supercooling and nucleation rate during the

202

water vapor condensation process. We can see that the supercooling degree increases

203

constantly along with the vapor expansion, and it rapidly rises to the peak value of

204

about 33 K in this case. In this condition, the steam is in an extremely

205

non-equilibrium thermodynamic state, leading to the occurrence of the spontaneous

206

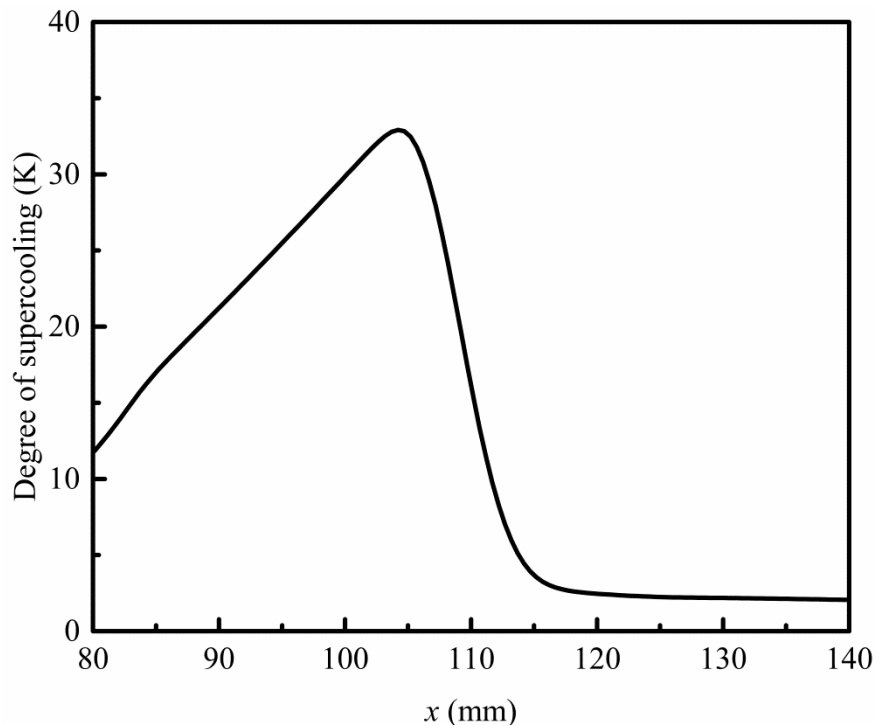
condensation in a very short moment, which can be observed in Fig. 9. The degree of

207

supercooling then suddenly decreases from 33 K to 2 K, which means that the

208 condensation process has finished.

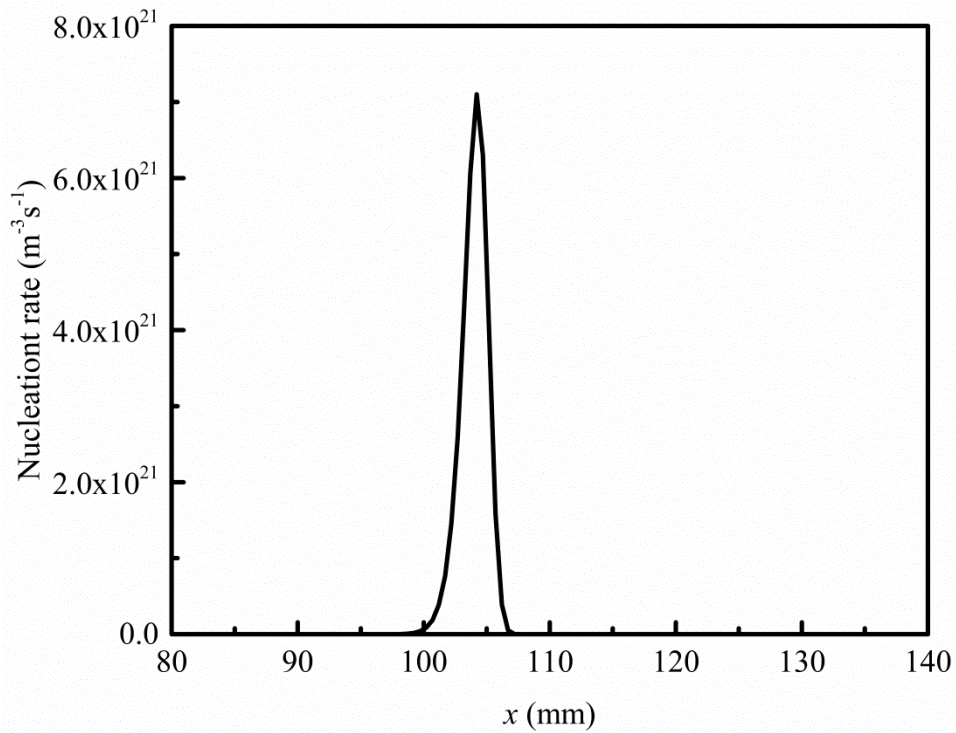
209 Fig. 9 obviously reflects the nucleation process of water vapor in supersonic
210 flows. The nucleation process starts to occur approximately at $x = 100$ mm, and
211 sharply rises from 0 to $7.2 \times 10^{21} \text{ m}^{-3} \text{ s}^{-1}$ in a very short time. It means that a massive
212 number of condensation nuclei appear in the steam. In a short while, the nucleation
213 rate drastically declines from peak to zero because of the decrease of the supercooling
214 degree. It indicates that the water vapor will not spontaneously condense at once when
215 the steam reaches the saturation state. On the contrary, the nucleation phenomenon
216 occurs somewhere downstream the nozzle throat, and shows a rapid variation both in
217 space and in time.



218

219 Fig. 8 Degree of supercooling at the central line of the Laval nozzle

220



221
222 Fig. 9 Nucleation rate at the central line of the Laval nozzle

223 The distribution of the droplet numbers at the center line of the Laval nozzle is
 224 shown in Fig. 10. The vapor molecules constantly collide with each other and
 225 coalesce, and continually produce the critical nucleus, when the spontaneous
 226 condensation starts to occur. Under this thermodynamic condition, a large number of
 227 droplets will appear when the condensation nucleus reaches a certain quantity and
 228 goes into the droplet growth process. The droplet numbers also rapidly rise from 0 to
 229 1.12×10^{17} in a very short distance due to the sharp process of the vapor nucleation.
 230 Then, the steam is almost back to the equilibrium state because of the decrease of the
 231 supercooling degree. At that moment, no new condensation nuclei appear and the
 232 droplet number remains effectively unchanged.

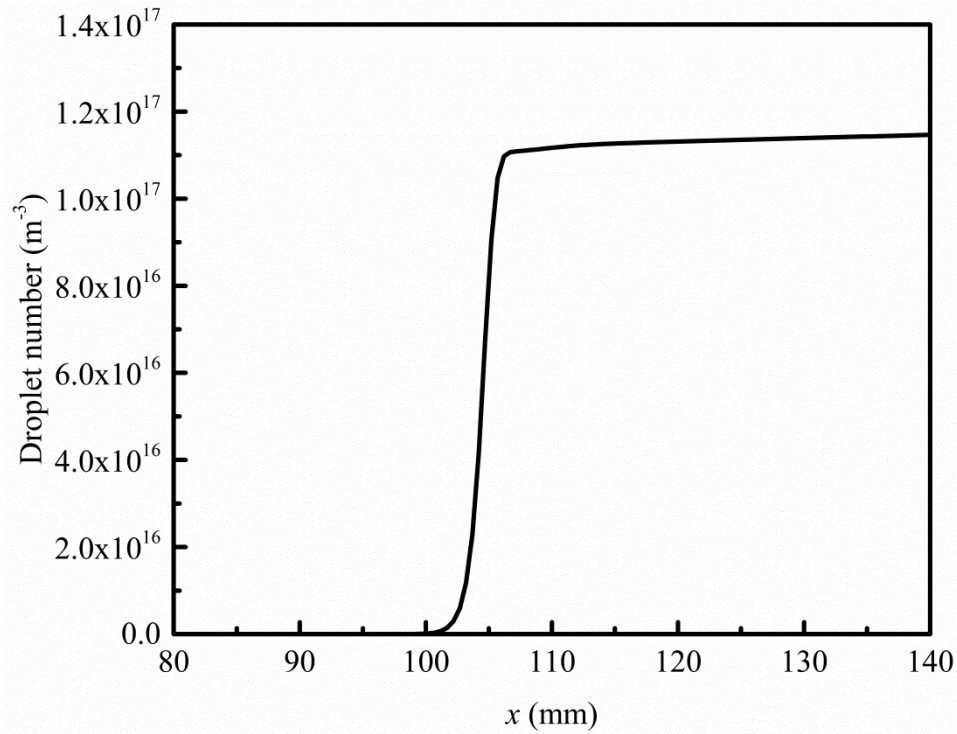
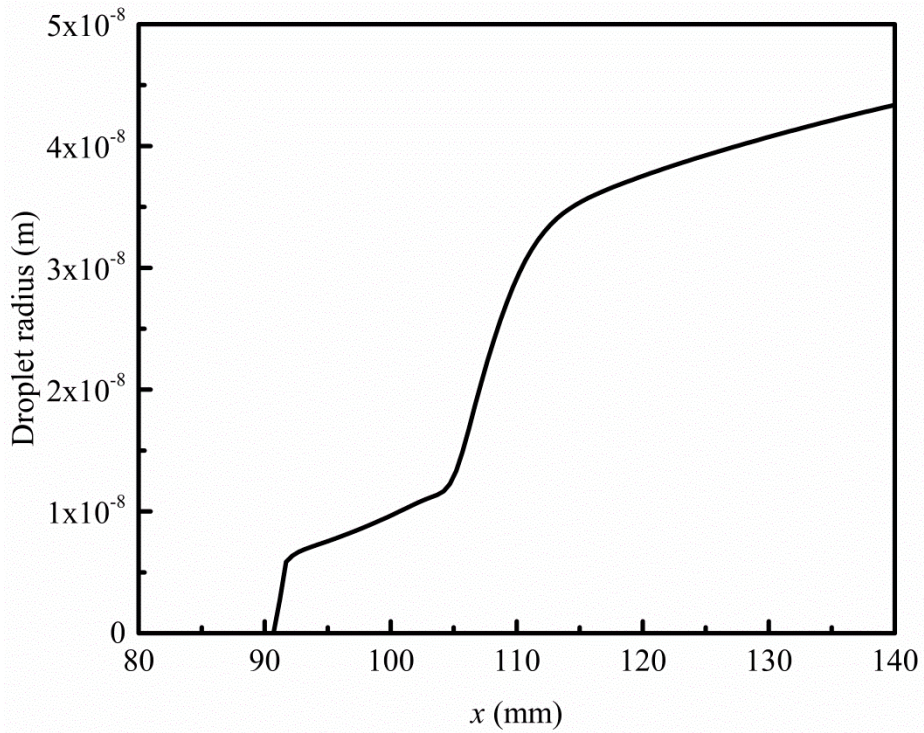


Fig. 10 Droplet numbers at the central line of the Laval nozzle

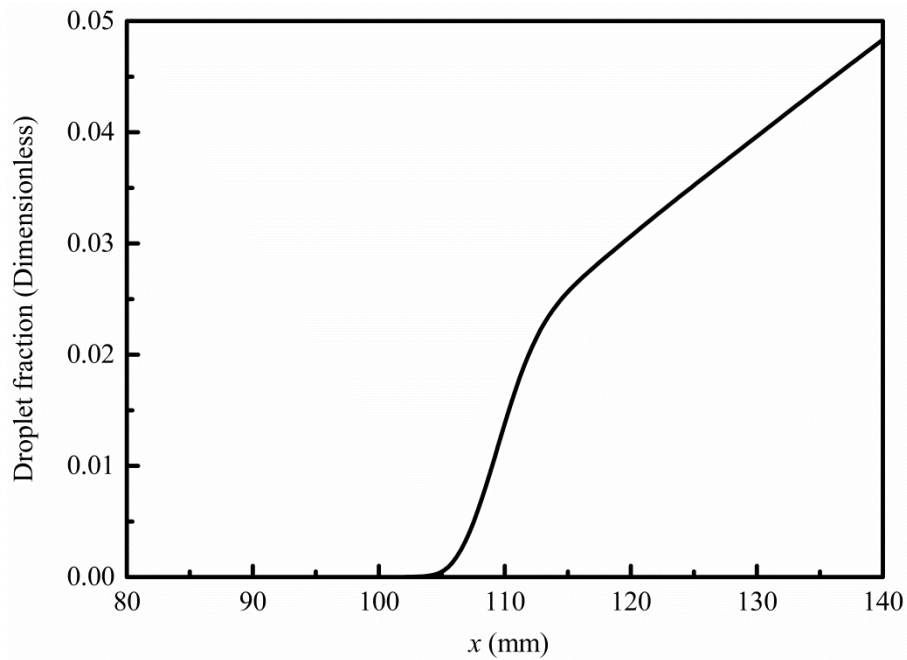
233
 234
 235 Figs. 11 and 12, respectively, show the radius and mass fraction of the droplet at
 236 the center line of the Laval nozzle. The large numbers of vapor molecules are able to
 237 aggregate on the droplet surface, when the nucleation rate and droplet numbers reach
 238 the peak. The radius and mass fraction of the droplet also begin to rapidly increase as
 239 a result of the large number of the condensing nuclei and droplet numbers. It also can
 240 be seen that the increase of the droplet mass fraction lags behind the change of the
 241 droplet radius by comparing Figs. 11 and 12. It means that the droplet radius changes
 242 in the first place and then the droplet fraction grows dramatically. Combining Figs. 8
 243 and 9, we also find that the vapor molecules can still continue to aggregate on the
 244 droplet surface due to the supercooling degree at about 2 K, when the droplet number
 245 remains unchanged. Therefore, the radius and mass fraction of the droplet increase
 246 continuously till the nozzle outlet as a result of the state of supersaturation.



247

248

Fig. 11 Droplet radius at the central line of the Laval nozzle



249

250

Fig. 12 Droplet fraction of at the central line of the Laval nozzle

251 **4. Conclusions**

252 The condensation process of water vapor in the Laval nozzle is simulated

253 numerically with the nucleation and droplet growth theories. The results show that the

254 latent heat is released to heat into the vapor phase during the spontaneous
255 condensation, leading to the jump of the condensing parameters. The degree of
256 supercooling can reach a maximum value of about 33 K and correspondingly the
257 spontaneous condensation occurs in a very short time. The droplet numbers also
258 rapidly rise from 0 to 1.12×10^{17} in a very short moment. Then, the radius and mass
259 fraction of the droplet also begin to increase continuously till the nozzle outlet as a
260 result of the supercooling degree at about 2 K.

261 **Acknowledgements**

262 This work was supported in part by the Natural Science Foundation of Jiangsu
263 Province, China (No. BK20150270), and the General Program of Natural Science
264 Research Project of Jiangsu Province Universities and Colleges (No. 15KJB440001).
265 C. Wen acknowledges the support of the H.C. Ørsted fellowship co-funded by Marie
266 Curie Actions at the Technical University of Denmark, DTU.

267 **References**

- 268 [1] S.J. Keisari, M. Shams, Shape optimization of nucleating wet-steam flow nozzle,
269 Appl. Therm. Eng. 103 (2016) 812-820.
- 270 [2] Y. Patel, G. Patel, T. Turunen-Saaresti, Influence of turbulence modelling on
271 non-equilibrium condensing flows in nozzle and turbine cascade, Int. J. Heat
272 Mass Transfer 88 (2015) 165-180.
- 273 [3] N. Sharifi, M. Boroomand, M. Sharifi, Numerical assessment of steam nucleation
274 on thermodynamic performance of steam ejectors, Appl. Therm. Eng. 52 (2013)
275 449-459.

-
- 276 [4] S.M.A. Noori Rahim Abadi, R. Kouhikamali, K. Atashkari, Non-equilibrium
277 condensation of wet steam flow within high-pressure thermo-compressor, *Appl.*
278 *Therm. Eng.* 81 (2015) 74-82.
- 279 [5] C. Wen, A. Li, J.H. Walther, Y. Yang, Effect of swirling device on flow behavior in
280 a supersonic separator for natural gas dehydration, *Sep. Purif. Technol.* 168 (2016)
281 68-73.
- 282 [6] C. Wen, Y. Yang, J.H. Walther, K.M. Pang, Y. Feng, Effect of delta wing on the
283 particle flow in a novel gas supersonic separator, *Powder Technol.* 304 (2016)
284 261-267.
- 285 [7] Y. Yang, A. Li, C. Wen, Optimization of static vanes in a supersonic separator for
286 gas purification, *Fuel Process. Technol.* 156 (2017) 265-270.
- 287 [8] Y. Yang, C. Wen, CFD modeling of particle behavior in supersonic flows with
288 strong swirls for gas separation, *Sep. Purif. Technol.* 174 (2017) 22-28.
- 289 [9] Y. Yang, C. Wen, S. Wang, Y. Feng, P. Witt, The swirling flow structure in
290 supersonic separators for natural gas dehydration, *RSC Adv.* 4 (2014)
291 52967-52972.
- 292 [10] S. Dykas, M. Majkut, M. Stozik, K. Smółka, Experimental study of condensing
293 steam flow in nozzles and linear blade cascade, *Int. J. Heat Mass Transfer* 80
294 (2015) 50-57.
- 295 [11] H. Ding, C. Wang, Y. Zhao, An analytical method for Wilson point in nozzle flow
296 with homogeneous nucleating, *Int. J. Heat Mass Transfer* 73 (2014) 586-594.
- 297 [12] C. Moses, G. Stein, On the growth of steam droplets formed in a Laval nozzle

298 using both static pressure and light scattering measurements, *J. Fluids Eng.* 100
299 (1978) 311-322.

300 [13] P.G. Hill, Condensation of water vapour during supersonic expansion in nozzles,
301 *J. Fluid Mech.* 25 (1966) 593-620.

302 [14] S.M.A. Noori Rahim Abadi, R. Kouhikamali, K. Atashkari, Two-fluid model for
303 simulation of supersonic flow of wet steam within high-pressure nozzles, *Int. J.*
304 *Therm. Sci.* 96 (2015) 173-182.

305 [15] A. White, J. Young, Time-marching method for the prediction of
306 two-dimensional, unsteady flows of condensing steam, *J. Propul. Power* 9 (1993)
307 579-587.

308 [16] A. Gerber, Two-phase Eulerian/Lagrangian model for nucleating steam flow, *J.*
309 *Fluids Eng.* 124 (2002) 465-475.

310 [17] M.R. Mahpeykar, A. Taymourtash, The effects of friction factor and inlet
311 stagnation conditions on the self condensation of steam in a supersonic nozzle,
312 *Sci. Iranica* 11 (2004) 269-284.

313 [18] W. Jiang, Z. Liu, H. Liu, H. Pang, L. Bao, Influences of friction drag on
314 spontaneous condensation in water vapor supersonic flows, *Sci. China Ser. E:*
315 *Technol. Sci.* 52 (2009) 2653-2659.

316 [19] D. Simpson, A. White, Viscous and unsteady flow calculations of condensing
317 steam in nozzles, *Int. J. Heat Fluid Flow* 26 (2005) 71-79.

318 [20] Y. Yang, S. Shen, Numerical simulation on non-equilibrium spontaneous
319 condensation in supersonic steam flow, *Int. Commun. Heat Mass Transfer* 36

-
- 320 (2009) 902-907.
- 321 [21] B. Nikkhahi, M. Shams, M. Ziabasharhagh, A numerical study of two-phase
322 transonic steam flow through convergence-divergence nozzles with different rates
323 of expansion, *Korean J. Chem. Eng.* 27 (2010) 1646-1653.
- 324 [22] S. Dykas, W. Wróblewski, Numerical modelling of steam condensing flow in low
325 and high-pressure nozzles, *Int. J. Heat Mass Transfer* 55 (2012) 6191-6199.
- 326 [23] A.H. Yousif, A.M. Al-Dabagh, R.C. Al-Zuhairy, Non-equilibrium spontaneous
327 condensation in transonic steam flow, *Int. J. Therm. Sci.* 68 (2013) 32-41.
- 328 [24] S.L. Girshick, C.P. Chiu, Kinetic nucleation theory: A new expression for the rate
329 of homogeneous nucleation from an ideal supersaturated vapor, *J. Chem. Phys.*
330 93 (1990) 1273-1277.
- 331 [25] G. Gyarmathy, The spherical droplet in gaseous carrier streams: review and
332 synthesis, *Multiphase Sci. Technol.* 1 (1982) 99-279.
- 333 [26] C. Wen, X. Cao, Y. Yang, Y. Feng, Prediction of mass flow rate in supersonic
334 natural gas processing, *Oil Gas Sci. Technol.* 70 (2015) 1101-1109.
- 335 [27] C. Wen, X. Cao, Y. Yang, W. Li, An unconventional supersonic liquefied
336 technology for natural gas, *Energy Educ. Sci. Technol. Part A Energy Sci. Res.* 30
337 (2012) 651-660.
- 338 [28] Y. Yang, C. Wen, S. Wang, Y. Feng, Numerical simulation of real gas flows in
339 natural gas supersonic separation processing, *J. Nat. Gas Sci. Eng.* 21 (2014)
340 829-836.
- 341 [29] Y. Yang, C. Wen, S. Wang, Y. Feng, Effect of Inlet and Outlet Flow Conditions on

342 Natural Gas Parameters in Supersonic Separation Process, PloS One 9 (2014)

343 e110313.

344 [30] F.R. Menter, Two-equation eddy-viscosity turbulence models for engineering

345 applications, AIAA J. 32 (1994) 1598-1605.

346 [31] S.V. Patankar, D.B. Spalding, A calculation procedure for heat, mass and

347 momentum transfer in three-dimensional parabolic flows, Int. J. Heat Mass

348 Transfer 15 (1972) 1787-1806.

349